Geophys. J. Int. (2004) **159,** 961–977 doi: 10.1111/j.1365-246X.2004.02401.x

Scattering of elastic waves in media with a random distribution of fluid-filled cavities: theory and numerical modelling

Tae-Kyung Hong* and B. L. N. Kennett

Research School of Earth Sciences, Institute of Advanced Studies, The Australian National University, Canberra, ACT 0200, *Australia*

Accepted 2004 June 3. Received 2004 March 10; in original form 2003 May 15

SUMMARY

The propagation of elastic waves is modelled in media with a random distribution of fluid-filled circular cavities, which display high physical impedance in contrast to background media. Theoretical attenuation expressions for media with circular cavities, which may be filled with any material (e.g. vacuum, fluid, elastic materials), are formulated using an ensemble treatment for first-order transmitted waves. Numerical estimates of scattering attenuation rates agree with the theoretical results well. The scattering attenuations (Q^{-1}) are proportional to the scale of cavities and the number density (η, number of cavities per area in a medium). The decrease of primary energy with the size of cavities does not result in the increase of coda energy owing to the increase of both purely backscattered waves from cavities and the trapped waves inside cavities. Scattering properties (e.g. scattering attenuation, coda energy, phase fluctuation of primary waves) in media with randomly distributed cavities are very different from those in stochastic random media. It appears that heterogeneities with high impedance in the earth may not be well represented with stochastic random heterogeneities.

Key words: attenuation, elastic waves, numerical modelling, scattering, single scattering theory, wavelet-based method.

1 INTRODUCTION

Since the pioneering work of Chernov (1960) which introduced a stochastic representation technique for random heterogeneities with smooth variation, many studies have implemented stochastic random media for the investigation of scattering of elastic or acoustic waves (e.g. Frankel & Clayton 1986; Roth & Korn 1993; Sato & Fehler 1998; Hong & Kennett 2003a; Hong 2004). As an alternative way to represent random heterogeneity, some studies (e.g. Yomogida & Benites 1995; Kawahara & Yamashita 1992) applied media composed of discrete uniform heterogeneities with random distribution and high physical impedance to the background, such as cracks or cavities.

Theoretical scattering attenuation rates for fracture zones with randomly distributed cracks (fluid filled or unfilled) were formulated by Kawahara & Yamashita (1992) by using the representation theorem for displacement discontinuity across the crack and the mean waveformalism (e.g. Hudson 1980) considering the average wavefield over the random media. The cracks are regarded as thin compared to both the length of the cracks and the wavelength of incident waves. The theoretical attenuation expressions of *SH* waves were compared with numerical results in 2-D media (Murai *et al.* 1995). The scattering attenuation rates depend on the state of the crack surfaces (e.g. viscous, dry) and are inversely proportional to wavenumber at large wavenumbers.

For investigation of scattering attenuation in media with a random distribution of cavities, however, theoretical scattering attenuation expression has not been formulated. Thus, numerical results (Benites *et al.* 1992; Yomogida & Benites 1995) have been compared with the theoretical attenuation curves for stochastic random media (e.g. Wu 1982). However, it is also unclear if the scattering pattern in the stochastic random media is identical or even comparable to that in media with randomly distributed cavities. Further, it is not certain which parameter in media with randomly distributed cavities corresponds to the perturbation strength of physical parameters in stochastic random media, which is an essential factor controlling both the scattering pattern and the level of scattering attenuation. Thus, for correct investigation, it is required to formulate theoretical attenuation expression for the media with a random distribution of cavities.

For numerical simulation in random media, many numerical techniques have been implemented. Finite difference methods (FDM) have been widely used for modelling in stochastic random media due to the simplicity in designing numerical models and codes (Frankel &

*Now at: Lamont-Doherty Earth Observatory, Columbia University. E-mail: tkhong@ldeo.columbia.edu.

Clayton 1986; Roth & Korn 1993). However, the accuracy limitation in numerical differentiation prevents the FDM from treating small-scale heterogeneities without the introduction of a dense grid system. Nagano (1998) applied the Haskell's matrix method (Haskell 1953) to analyse the crack waves trapped inside a single fracture which is layered horizontally between low-velocity layers. However, this class of methods is limited to simplified layered-structure problems, and thus it is difficult to take into consideration of micro-structures properly. Another different attempt in numerical simulation is to use the indirect boundary element method (IBEM). Pointer *et al.* (1998) implemented the IBEM for modelling of elastic waves in media with single crack and studied the pattern of diffraction and scattering at various crack lengths, crack opening sizes and filling materials. Carcione (1998) used a pseudospectral Chebyshev method for the single-cracked media. However, the technique inhibits incorporation of heterogeneities in various sizes and shapes without an interpolation procedure.

In order to consider cracks and cavities of complex shape, several alternative numerical techniques have been introduced. Murai *et al.* (1995) used the representation theorem (Pao & Mow 1973) in building a 2-D *SH* wavefield at fracture zones where uniform cracks are aligned parallel each other. Liu *et al.* (1997) implemented the Kirchhoff approximation technique, which requires a small computational cost compared to classical grid-based methods, for the investigation of diffraction and scattering of 3-D elastic waves in media with a single crack. Also, boundary integral methods (Coutant 1989; Yomogida & Benites 2002, 1995) were employed for modelling in media with random cracks (or cavities). However, although these semi-analytic techniques allow accurate modelling in media with cavities of complex shape, it is very hard to expand them to problems with heterogeneous background media (random physical perturbation or layered structure) due to the difficulty in obtaining a Green's function for such media. Further, when the shapes of cracks or cavities are complicated, the computational cost increases significantly. Also, when the cracks (or cavities) are filled with elastic or fluid materials, additional computational efforts are required to compute the internal waves inside the cracks and cavities.

We implement a wavelet-based method (Hong & Kennett 2002a,b, 2003b), which allows high accuracy and stability for modelling even in media composed of small-scale heterogeneities with high impedance to background. We measure scattering attenuation rates of elastic waves in random fluid-filled cavity media, and investigate the scattering properties of elastic waves in the media. In order to formulate theoretical attenuation expressions for media with randomly distributed cavities, we use an analytic wavefield in media with a single circular crack (Pao & Mow 1973) and calculate stochastic wavefield for media with randomly distributed cavities through an ensemble treatment of first-order transmitted waves. An autocorrelation function for the representation of cavity distribution in spatial domain is determined through numerical experiments. We compare the theoretical attenuation curve with with numerical results estimated from time responses. Differences in theoretical attenuation variations between stochastic random media and random cavity media are discussed, and characteristics of both media are compared.

2 NUMERICAL MODELLING AND SCATTERING FEATURES

We have investigated the scattering of elastic waves in stochastic random media in Hong & Kennett (2003a) and Hong (2004). As an alternative representation of random media, media composed of randomly distributed homogeneous heterogeneities with high impedance to background (e.g. cracks and cavities) have been considered. We consider media with fluid-filled cavities and investigate difference in wavefields and scattering properties between stochastic random media and random cavity media. For numerical modelling, we use a wavelet-based method (Hong & Kennett 2002a,b, 2003b) which has high stability and accuracy even in highly perturbed media.

We first simulate elastic wave propagation in a medium with a fluid-filled circular cavity. Wave velocities in the background medium are 3.6 km s^{-1} for *P* waves and 2.06 km s^{-1} for *S* waves, and the density is 2.4 g cm^{-3}. The physical parameters of the fluid in the cavity are 1.8 km s^{-1} for *P* waves and 1.2 g cm^{-3} for the density, but the shear wave velocity is zero. The radius of the cavity is 0.47 km. Plane *P* waves with dominant frequency of 4.5 Hz are incident in the vertical direction from the bottom. Fig. 1 shows successive snapshots of the wavefield. The snapshot for $t = 2.0$ s clearly displays the dimension of the cavity. Diffracted coupled *P* and *S* waves develop from the boundary of the cavity where the plane *P* waves are incident, and only *P* waves are transmitted inside the cavity. The transmitted waves are multiply reflected inside the cavity and successive multi-order coupled waves follow the diffracted waves. The secondary phases are displayed clearly in the *x*-component snapshots where primary waves are not recorded. After sweeping the cavity area, phase healing in the primary wave front (e.g. Igel & Gudmundsson 1997) occurs as it propagates through the homogeneous background. We find that the amplitudes of primary wave front change smoothly over a wide range (see the *z*-component snapshots for $t = 2.0$ and 3.0 s). Even after a long time lapse, interference of the internal fluid waves is still clearly shown (see the snapshot for $t = 3.5$ s).

We now investigate the scattering properties of elastic waves in media with randomly distributed cavities. Cavities are distributed randomly inside a cavity zone (40 km-by-17.2 km in Fig. 2) with homogeneous background media (40 km-by-23.8 km). Scattering properties in media with randomly distributed cavities are expected to be dependent on both the number and the scale of the cavities. We first consider a constant number of cavities, $N_c = 22$. Two different numbers of cavities ($N_c = 89$, 112) are considered additionally for the investigation of the change in scattering properties and for the verification of theoretical attenuation expression.

The positions of cavities are set consistent for various cavity radii. When more cavities (i.e. $N_c = 89$, 112) are considered in media, additional random positions are implemented. Fig. 2 shows the location of cavities in media. The wave speeds in the medium are $\alpha_0 = 3.15$ km s^{-1} and $\beta_0 = 1.8$ km s^{-1}, and the density is $\rho_0 = 2.2$ g cm^{-3}. Also, the *P* wave velocity (α_f) and the density (ρ_f) in the cavities are half those in background media, and the shear wave velocity (β_f) is zero. Plane *P* waves are incident to the bottom of the cavity zone. The source time function is the Ricker wavelet with dominant frequency of 4.5 Hz. The domain is represented by 512-by-220 gridpoints and the grid step

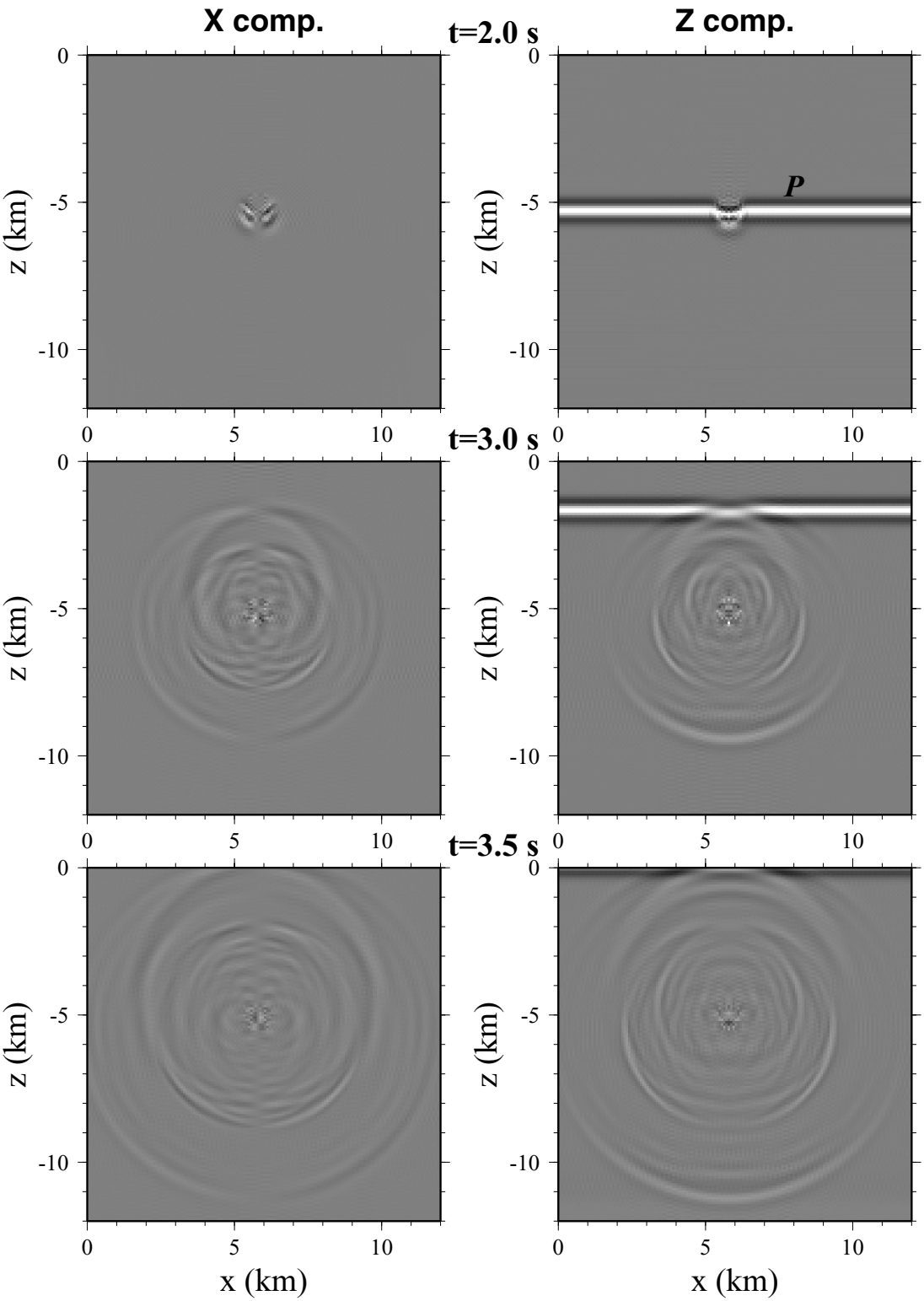

Figure 1. Snapshots of displacement wavefield for a plane *P* wave incidence in a medium with a fluid-filled cavity at $t = 2.0$, 3.0 and 3.5 s. The source time function of incident waves is the Ricker wavelet with dominant frequency of 4.5 Hz. Diffracted and reflected waves are successively generated.

$(\delta x, \delta z)$ is 78.1 m. 128 receivers are placed on the top of media with a uniform interval of 312.4 m. The two vertical artificial boundaries (Γ_R, Γ_L) are considered with periodic boundary conditions to satisfy with the condition for homogeneous distribution of cavities inside the medium and to model media with a horizontally unbounded cavity zone. For stable numerical modelling using a wavelet-based method, the numerical domain is designed to satisfy the required conditions, e.g. the wavelength of the slowest phase compared to the grid step and the discrete time step depending the highest velocity in domain (see Hong & Kennett 2002a,b).

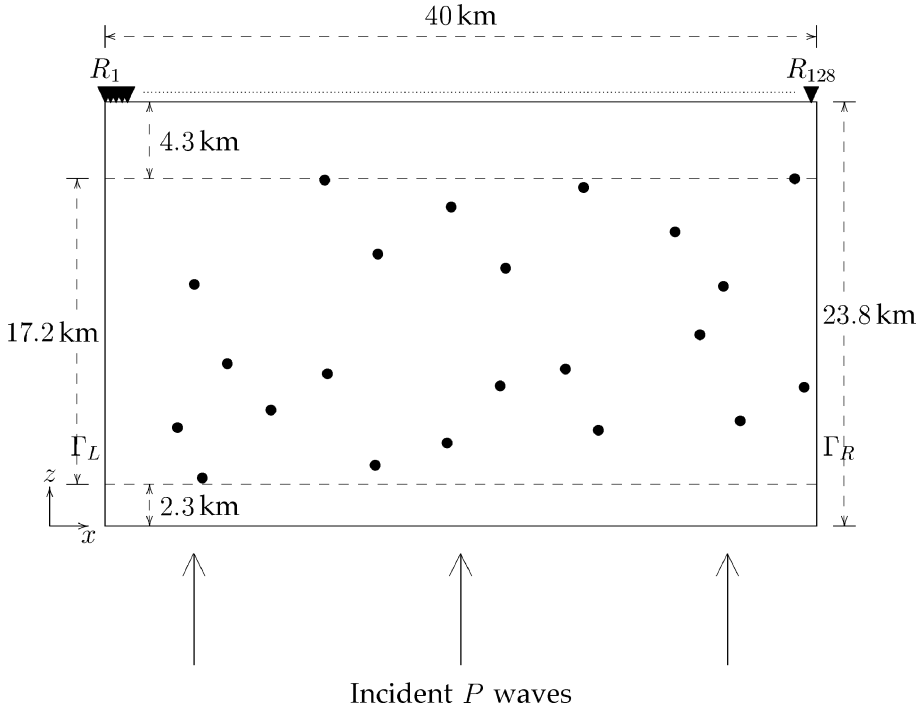

Figure 2. Representation of a domain (40 km-by-23.8 km) with a random distribution of 22 fluid-filled cavities. The cavities are distributed in a confined region (40 km-by-17.2 km) and 128 receivers (R_j) are placed at the top boundary of the domain. For domains with 89 or 112 cavities, additional random positions are included to the given 22 cavity positions. Plane *P* waves are incident from the bottom of domain. The left and right artificial boundaries (Γ_L, Γ_R) are considered with periodic boundary conditions to satisfy with the condition for homogeneous distribution of cavity in a medium.

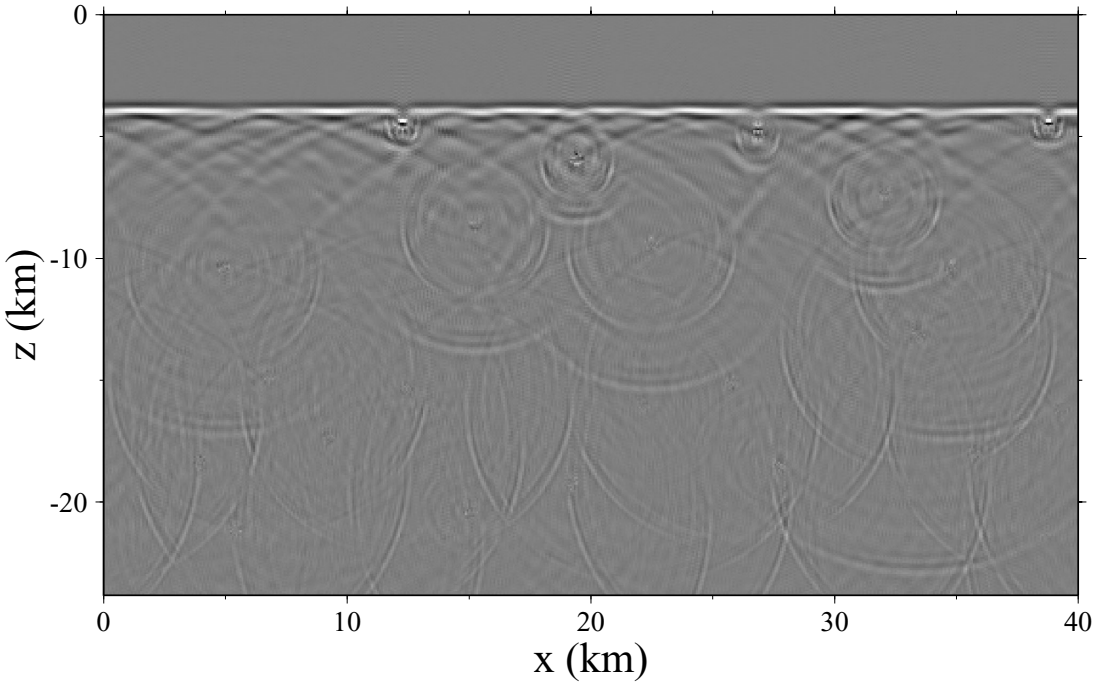

Figure 3. Snapshot of displacement wavefield for a plane *P* wave incidence in a medium with 22 fluid-filled cavities at $t = 6.5$ s. The radius of the cavities are 312 m. Wave type coupled circular diffracted waves are generated from cavities. The waves trapped inside cavities leak energy continuously during the internal multiscattering. The energy of primary waves is distributed homogeneously along the primary wave front during propagation in the homogeneous background media.

A snapshot of the displacement wavefield at $t = 6.5$ s in a medium with 22 fluid-filled cavities with a radius of 312 m is shown in Fig. 3. Reflected and diffracted waves from the cavities follow after the primary plane *P* waves. Multi-order secondary waves develop continuously from the boundaries of cavities. Magnitudes of scattered waves increase with the size and the number of cavities due to the high impedance contrast on cavity boundaries. However, the magnitude of coda waves does not increase much in the media with large scale or number of

cavities since purely backscattered waves (waves reflected in the reverse direction) do not arrive at receivers which are placed over the cavity zone (see Fig. 4). This feature is related to the presence of discrete heterogeneities with high impedance to background. That is, a significant portion of incident energy waves are blocked by cavities, and are reflected back (propagating reversely). Backscattered waves thus become stronger and multiply-scattered waves are distributed homogeneously in media. This is a characteristic feature which is different from that in stochastic random media; purely backscattered waves are not strong in stochastic random media since the fluctuation of perturbation changes gradually.

The traveltime anomaly in time responses is not significant even in media with a large size and number of cavities, since primary waves are composed mainly of forward diffracted waves and energy complemented from the adjacent primary wave front. Note that the waves transmitting through fluid-filled cavities lose energy significantly by multiple energy division (at least twice) on the cavity boundaries. Thus, the transmitting waves exhibit a small amplitude and hardly influence the primary wave front. Moreover, the velocity difference between inside and outside cavity prevents the transmitted energy from joining in primary waves. On the other hand, the forward diffracted waves over cavities which propagate within a small angle of the incident direction, join in the primary-wave portion. The diffracted waves with a large propagation angle from the incident direction are separated from the primary wave front and do not make influence on the primary-wave portion at receivers placed at a large horizontal distance from the cavity. It is noteworthy that the wave fronts in media with fluid-filled cavities do not have a faster traveltime since the cavities have only reduced wave velocities, while those in stochastic media display phase fluctuation over the reference traveltime.

Along with snapshots in Fig. 1, time responses show that the primary waves are recorded mainly on the z component regardless of the scale and the number of cavities. The wavefield pattern is different from that in stochastic random media with large scale of heterogeneities, where primary waves are recorded on both x and z components by the influence of refraction.

3 FORMULATION OF THEORETICAL SCATTERING ATTENUATION EXPRESSION

We formulate an analytical expression for scattering attenuation of P waves (Q^{-1}) in media with randomly distributed cavities. We consider a medium with a cavity with a radius of a_c. Here the medium can be regarded as a sum of two domains, Ω_0 (medium except the inclusion) and Ω_1 (inside the cavity). The P and S wave velocities in Ω_0 are α_0 and β_0, and those in Ω_1 are α_1 and β_1. When the centre of the cavity is located at the origin ($\mathbf{0}$) of a coordinate system, the displacement potential at $\mathbf{x}$ for vertically incident unit P waves (Φ^{i}) is given by (Pao & Mow 1973; Liu *et al.* 2000)

$$\Phi^{\mathrm{i}}(\mathbf{x};\mathbf{0}) = \exp\left[i(k_\alpha z - \omega t)\right] = \sum_{m=0}^{\infty} i^m \epsilon_m J_m(k_\alpha r)\cos(m\phi)e^{-i\omega t}, \tag{1}$$

where k_α is the wavenumber of the incident P waves with velocity α_0, J_m is the Bessel function of the first kind of order m and ϵ_m is a Neumann factor given by $\epsilon_0 = 1$ and $\epsilon_j = 2$ for $j \geq 1$. The angle ϕ is measured from z axis and therefore $\mathbf{x}$ is given by ($r\,\sin\phi, r\,\cos\phi$).

The displacement potentials for scattering waves (Φ^{s}, Ψ^{s}) outside the inclusion region are given by

$$\Phi^{\mathrm{s}}(\mathbf{x};\mathbf{0}) = \sum_{m=0}^{\infty} i^m \epsilon_m A_m H_m^{(1)}(k_\alpha r)\cos(m\phi)e^{-i\omega t},$$

$$\Psi^{\mathrm{s}}(\mathbf{x};\mathbf{0}) = \sum_{m=0}^{\infty} i^{m+1} \epsilon_m B_m H_m^{(1)}(k_\beta r)\sin(m\phi)e^{-i\omega t}, \tag{2}$$

and the transmitted waves (Φ^{f}, Ψ^{f}) inside the inclusion are

$$\Phi^{\mathrm{f}}(\mathbf{x};\mathbf{0}) = \sum_{m=0}^{\infty} i^{m+1} \epsilon_m C_m J_m^{(1)}(k_{\alpha_2} r)\cos(m\phi)e^{-i\omega t},$$

$$\Psi^{\mathrm{f}}(\mathbf{x};\mathbf{0}) = \sum_{m=0}^{\infty} i^{m+1} \epsilon_m D_m J_m^{(1)}(k_{\beta_2} r)\sin(m\phi)e^{-i\omega t}, \tag{3}$$

where k_β is the wavenumber of S waves, $H_m^{(1)}$ is a Hankel function of the first kind of order m, and A_m, B_m, C_m and D_m are unknown complex-value constants given by

$$A_m = -\frac{K_1(m)}{K_0(m)}, \quad B_m = -\frac{2}{\pi}\frac{K_2(m)}{K_0(m)}, \quad C_m = -\frac{2}{\pi}\frac{K_3(m)}{K_0(m)}, \quad D_m = -\frac{2}{\pi}\frac{K_4(m)}{K_0(m)}, \tag{4}$$

and the K_j ($j = 0, 1, 2, 3, 4$) are determined by the boundary conditions of the inclusion (Pao & Mow 1973). The boundary conditions (continuity of displacement, continuity of stress at the boundary) are varied following the material of the inclusion. Simplified formulation of K_j is given in Liu *et al.* (2000).

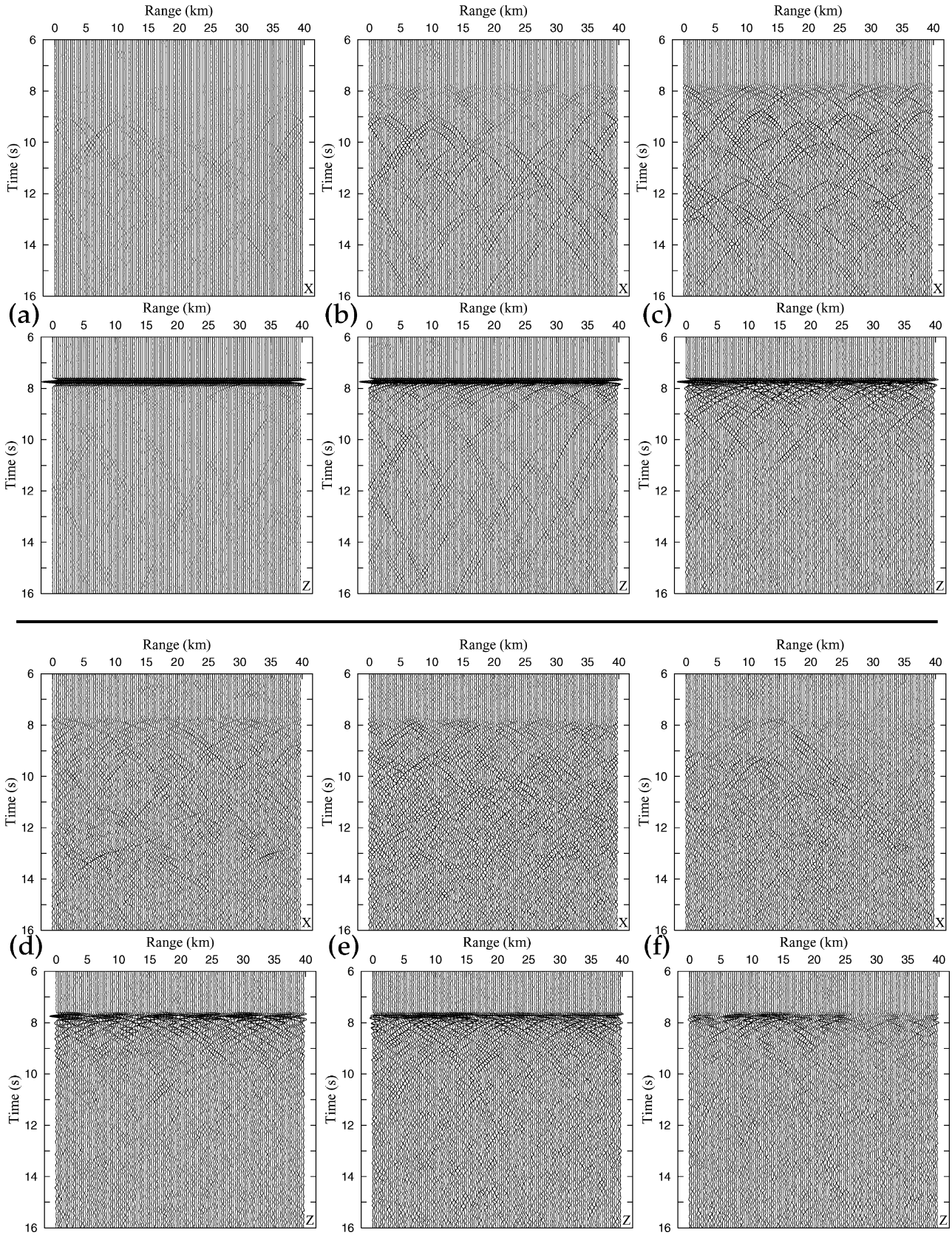

Figure 4. Time responses recorded at the 112 receivers (R_j, $j = 1, 2, \ldots, 128$ in Fig. 2) in media composed of (a) 22 cavities with a radius (a_c) of 39 m, (b) 22 cavities with $a_c = 94$ m, (c) 22 cavities with $a_c = 234$ m, (d) 22 cavities with $a_c = 625$ m, (e) 89 cavities with $a_c = 156$ m, and (f) 112 cavities with $a_c = 312$ m. With increase of the number and the radius of cavities, the energy loss of the incident waves increases. Also, scattered waves are distributed homogeneously at the receivers regardless of the scale and the number of the cavities.

The displacement and the stress components can be represented in terms of potentials by

$$
\begin{aligned}
u_r^j &= \frac{\partial \Phi^j}{\partial r} + \frac{1}{r}\frac{\partial \Psi^j}{\partial \theta}, \qquad u_\theta^j = \frac{1}{r}\frac{\partial \Phi^j}{\partial \theta} - \frac{\partial \Psi^j}{\partial r},\\
\sigma_{rr}^j &= (\lambda + 2\mu)\frac{\partial^2 \Phi^j}{\partial r^2} + \frac{\lambda}{r}\frac{\partial \Phi^j}{\partial r} + \frac{\lambda}{r^2}\frac{\partial^2 \Phi^j}{\partial \theta^2} - \frac{2\mu}{r^2}\frac{\partial \Psi^j}{\partial \theta} + \frac{2\mu}{r}\frac{\partial^2 \Psi^j}{\partial r \partial \theta},\\
\sigma_{\theta\theta}^j &= \frac{\lambda + 2\mu}{r^2}\frac{\partial^2 \Phi^j}{\partial \theta^2} + \lambda\frac{\partial^2 \Phi^j}{\partial r^2} + \frac{\lambda + 2\mu}{r}\frac{\partial \Phi^j}{\partial r} - \frac{2\mu}{r}\frac{\partial^2 \Psi^j}{\partial r \partial \theta} + \frac{2\mu}{r^2}\frac{\partial \Psi^j}{\partial \theta},\\
\sigma_{r\theta}^j &= \frac{2\mu}{r}\frac{\partial^2 \Phi^j}{\partial r \partial \theta} - \frac{2\mu}{r^2}\frac{\partial \Phi^j}{\partial \theta} + \frac{\mu}{r^2}\frac{\partial^2 \Psi^j}{\partial \theta^2} - \mu\frac{\partial^2 \Psi^j}{\partial r^2} + \frac{\mu}{r}\frac{\partial \Psi^j}{\partial r},
\end{aligned}
\tag{5}
$$

where $j = 0, 1$ which denotes the domain (i.e. Ω_0 Ω_1). Thus, the potential wavefield in domain Ω_0 (Φ^0) can be represented by the sum of the incident wave potential and scattered (or refracted) wave potential ($\Phi^{\mathrm{i}} + \Phi^{\mathrm{s}}$).

Using the relationships $i^{-m} J_{-m}(x) = i^m J_m(x)$ and $i^{-m} H_{-m}(x) = i^m H_m(x)$ (*cf.* Arfken 1985), eqs (1) and (2) can be rewritten as

$$
\Phi^{\mathrm{i}}(\mathbf{x}; \mathbf{0}) = \sum_{m=-\infty}^{\infty} i^m J_m(k_\alpha r)\cos(m\phi) e^{-i\omega t},
\tag{6}
$$

and

$$
\begin{aligned}
\Phi^{\mathrm{s}}(\mathbf{x}; \mathbf{0}) &= \sum_{m=-\infty}^{\infty} i^m \mathcal{A}_m H_m^{(1)}(k_\alpha r)\cos(m\phi) e^{-i\omega t},\\
\Psi^{\mathrm{s}}(\mathbf{x}; \mathbf{0}) &= \sum_{m=-\infty}^{\infty} i^{m+1} \mathcal{B}_m H_m^{(1)}(k_\beta r)\sin(m\phi) e^{-i\omega t},
\end{aligned}
\tag{7}
$$

where $\mathcal{A}_m$ and $\mathcal{B}_m$ are

$$
\begin{aligned}
\mathcal{A}_m &= A_p, \quad p = |m|,\\
\mathcal{B}_m &= \begin{cases} B_p, & m \geq 0 \\ -B_p, & m < 0. \end{cases}
\end{aligned}
\tag{8}
$$

Since $\mathcal{A}_{-m}\sin(-m\phi) = -\mathcal{A}_m \sin(m\phi)$ and $\mathcal{B}_{-m}\cos(-m\phi) = -\mathcal{B}_m \cos(m\phi)$, we can include $\sin(m\phi)$ and $\cos(m\phi)$ additionally at (7) for convenience in treatment:

$$
\begin{aligned}
\Phi^{\mathrm{s}}(\mathbf{x}; \mathbf{0}) &= \sum_{m=-\infty}^{\infty} i^m \mathcal{A}_m H_m^{(1)}(k_\alpha r)\{\cos(m\phi) + i\sin(m\phi)\} e^{-i\omega t}\\
&= \sum_{m=-\infty}^{\infty} i^m \mathcal{A}_m H_m^{(1)}(k_\alpha r) e^{i(m\phi - \omega t)},\\
\Psi^{\mathrm{s}}(\mathbf{x}; \mathbf{0}) &= \sum_{m=-\infty}^{\infty} i^m \mathcal{B}_m H_m^{(1)}(k_\beta r)\{\cos(m\phi) + i\sin(m\phi)\} e^{-i\omega t}\\
&= \sum_{m=-\infty}^{\infty} i^m \mathcal{B}_m H_m^{(1)}(k_\beta r) e^{i(m\phi - \omega t)}.
\end{aligned}
\tag{9}
$$

We now consider the wavefield in media with randomly distributed cavities with a given radius. The media are sufficiently large and bear N_c cavities with a radius of a_c. The cavities are assumed to be distributed homogeneously and take a tiny area compared to the whole medium (S), i.e. $N_c a_c^2 \ll \mathsf{S}$. The total wavefield (Φ^{t}) recorded at a given receiver can be computed by integrating the waves propagating from all cavities. The influence of multiscattering between cavities is ignored by the assumption that cavities are distributed homogeneously in media and the distances between cavities are sufficiently large, as considered in a single scattering approximation (Wu 1982; Roth & Korn 1993).

For simplicity in treatment, we set the reference coordinate system at the receiver position, and this causes an angular transformation of θ in analytic expressions (9) as $\theta = \pi/2 + \phi$ (see Fig. 5). Also, we introduce 'location map' $R(\mathbf{x})$ for the representation of cavity distribution in media; the value of $R(\mathbf{x})$ is set to be 1 at locations of cavities ($\mathbf{x}_j^c$, $j = 1, 2, \ldots, N_c$) and zero elsewhere:

$$
R(\mathbf{x}) = \sum_{j=1}^{N_c} \delta\left(\mathbf{x} - \mathbf{x}_j^c\right),
\tag{10}
$$

where N_c is the number of cavities employed in media. Considering relative position for the location of a cavity centre ($\mathbf{x}^c$), the displacement potential $\Phi(\mathbf{x}; \mathbf{0})$ can be written by $\Phi(\mathbf{x} + \mathbf{x}^c; \mathbf{x}^c)$ for example. Therefore, the total wavefields from cavities can be written as

$$
\begin{aligned}
\Phi_a^{\mathrm{s}}(\mathbf{x}) &= \sum_{j=1}^{N_c} \Phi_j^{\mathrm{s}}(\mathbf{x}) = \sum_{j=1}^{N_c} \int_{\mathsf{S}} \Phi^{\mathrm{s}}\left(\mathbf{x}; \mathbf{x}_j^c\right) d\mathsf{S}\left(\mathbf{x}_j^c\right),\\
\Psi_a^{\mathrm{s}}(\mathbf{x}) &= \sum_{j=1}^{N_c} \Psi_j^{\mathrm{s}}(\mathbf{x}) = \sum_{j=1}^{N_c} \int_{\mathsf{S}} \Psi^{\mathrm{s}}(\mathbf{x})\left(\mathbf{x}; \mathbf{x}_j^c\right) d\mathsf{S}\left(\mathbf{x}_j^c\right).
\end{aligned}
\tag{11}
$$

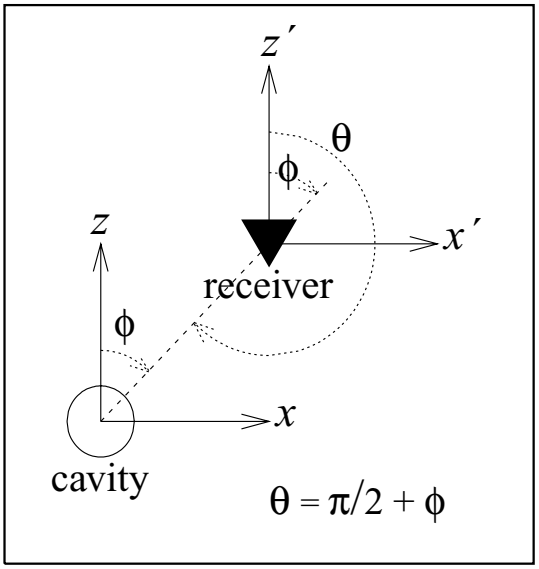

Figure 5. Change of reference axis centring from cavity to receiver and a related angle change from ϕ to θ.

Using an asymptotic expression for the Hankel function (Arfken 1985), we can rewrite the Hankel function, $H_m^{(1)}$ as

$$H_m^{(1)}(x) \approx \sqrt{\frac{2}{\pi x}} \exp\left[i\left(x - \frac{\pi}{4} - \frac{m\pi}{2}\right)\right]. \tag{12}$$

Since the receiver is assumed to be placed at large distances from scatterers (i.e. $|\mathbf{x}| \gg |\mathbf{x}_j^c|$), r_j ($=|\mathbf{x} - \mathbf{x}_j^c|$) in Fig. 6 can be given by $|\mathbf{x}| - \mathbf{n} \cdot \mathbf{x}_j^c$ where $\mathbf{n}$ is the unit vector in $\mathbf{x}$ direction. Also, $1/r_j$ can be approximated by $|\mathbf{x}|$ (e.g. Frankel & Clayton 1986). Thus, from (9) and (12), $\Phi_j^s(\mathbf{x})$ and $\Psi_j^s(\mathbf{x})$ in (11) can be written as

$$\Phi_j^s(\mathbf{x}) = \int_S \left\{ \sum_{m=-\infty}^{\infty} i^m \mathcal{A}_m \sqrt{\frac{2}{\pi k_\alpha |\mathbf{x}|}} \times \exp\left[i\left(k_\alpha |\mathbf{x}| - k_\alpha \mathbf{n} \cdot \mathbf{x}_j^c - \frac{\pi}{4} - \frac{m\pi}{2} + m\phi - \omega t\right)\right]\right\} dS(\mathbf{x}_j^c),$$

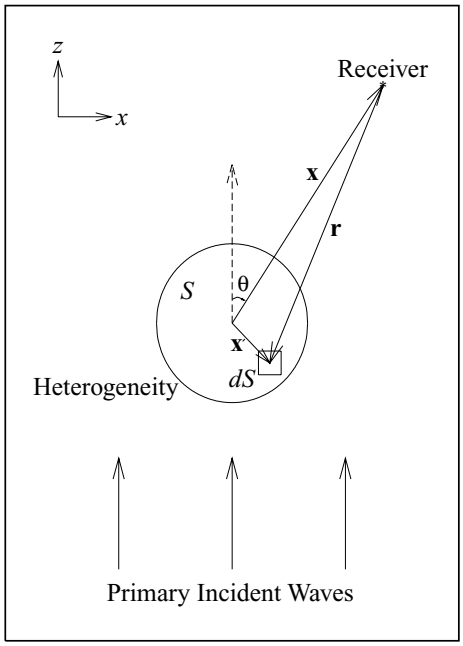

Figure 6. The scattering of the primary incident waves at the scatterer dS, a part of the whole heterogeneous area S. θ is the scattering angle from the incident direction of primary waves along the z axis. $\mathbf{x}$, $\mathbf{x}'$ are the location vectors for the receiver and a scatterer, and vector $\mathbf{r}$ links the scatterer to the receiver.

$$\Psi_j^{\mathrm{s}}(\mathbf{x}) = \int_{\mathsf{S}} \left\{ \sum_{m=-\infty}^{\infty} i^m \mathcal{B}_m \sqrt{\frac{2}{\pi k_\beta |\mathbf{x}|}} \times \exp\left[i \left(k_\beta |\mathbf{x}| - k_\beta \mathbf{n} \cdot \mathbf{x}_j^c - \frac{\pi}{4} - \frac{m\pi}{2} + m\phi - \omega t \right) \right] \right\} d\mathsf{S}(\mathbf{x}_j^c). \tag{13}$$

The expression in (13) can be simplified using a relationship of $\exp(-im\pi/2) = (-i)^m$ to give

$$\begin{aligned}
\Phi_j^{\mathrm{s}}(\mathbf{x}) &= \sum_{m=-\infty}^{\infty} \mathcal{A}_m \sqrt{\frac{2}{\pi k_\alpha |\mathbf{x}|}} \exp\left[i \left(k_\alpha |\mathbf{x}| - \omega t - \frac{\pi}{4} \right) \right] \\
&\quad \times \int_{\mathsf{S}} \exp\left[i \left(m\phi - k_\alpha \mathbf{n} \cdot \mathbf{x}_j^c \right) \right] d\mathsf{S}(\mathbf{x}_j^c) \\
\Psi_j^{\mathrm{s}}(\mathbf{x}) &= \sum_{m=-\infty}^{\infty} \mathcal{B}_m \sqrt{\frac{2}{\pi k_\beta |\mathbf{x}|}} \exp\left[i \left(k_\beta |\mathbf{x}| - \omega t - \frac{\pi}{4} \right) \right] \\
&\quad \times \int_{\mathsf{S}} \exp\left[i (m\phi - k_\beta \mathbf{n} \cdot \mathbf{x}_j^c) \right] d\mathsf{S}(\mathbf{x}_j^c),
\end{aligned} \tag{14}$$

where ϕ is the angular distance from the reference position ($\mathbf{x}$) to a scatterer's position ($\mathbf{x}_j^c$).

In order to compute average energy attenuation due to scattering, we consider an ensemble average of Φ_a^{s} and Ψ_a^{s}:

$$\begin{aligned}
\left\langle \left| \Phi_a^{\mathrm{s}} \right|^2 \right\rangle &= \frac{2N_c}{\pi k_\alpha |\mathbf{x}|} \sum_{m=-\infty}^{\infty} (\mathcal{A}_m)^2 \\
&\quad \times \int_{\mathsf{S}} \int_{\mathsf{S}} \langle R(\mathbf{x}) R(\mathbf{y}) \rangle \exp\left[i \left\{ m(\phi_{\mathbf{x}} - \phi_{\mathbf{y}}) - k_{\alpha_1} \mathbf{n} \cdot \left(\mathbf{x}_j^c - \mathbf{y}_j^c \right) \right\} \right] d\mathsf{S}(\mathbf{x}_j^c)\, d\mathsf{S}\left(\mathbf{y}_j^c \right), \\
\left\langle \left| \Psi_a^{\mathrm{s}} \right|^2 \right\rangle &= \frac{2N_c}{\pi k_\beta |\mathbf{x}|} \sum_{m=-\infty}^{\infty} (\mathcal{B}_m)^2 \\
&\quad \times \int_{\mathsf{S}} \int_{\mathsf{S}} \langle R(\mathbf{x}) R(\mathbf{y}) \rangle \exp\left[i \left\{ m(\phi_{\mathbf{x}} - \phi_{\mathbf{y}}) - k_{\beta_1} \mathbf{n} \cdot (\mathbf{x}_j^c - \mathbf{y}_j^c) \right\} \right] d\mathsf{S}(\mathbf{x}_j^c)\, d\mathsf{S}\left(\mathbf{y}_j^c \right).
\end{aligned} \tag{15}$$

We introduce new variables $\mathbf{p}$ for the centre-of-mass coordinate variable and $\mathbf{q}$ for the relative coordinate variable (e.g. Frankel & Clayton 1986):

$$\mathbf{p} = \left(\mathbf{x}_j^c + \mathbf{y}_j^c \right)/2, \qquad \mathbf{q} = \mathbf{x}_j^c - \mathbf{y}_j^c. \tag{16}$$

When we consider the integrals in (15) with the new variables ($\mathbf{p}$, $\mathbf{q}$), the integration for $\mathbf{p}$ yields the area S and the integration for $\mathbf{q}$ can be considered simply in a polar coordinate system (r', ϕ') using the relationship

$$r' = |\mathbf{q}|, \qquad \phi' = \phi_{\mathbf{x}} - \phi_{\mathbf{y}}, \qquad d\mathsf{S}(\mathbf{q}) = r' dr' d\phi'. \tag{17}$$

The resultant ensemble averages, then, can be simplified with additional introduction of an autocorrelation function $N(r')$ for stochastic representation of the location map $R(\mathbf{x})$:

$$\begin{aligned}
\left\langle \left| \Phi_a^{\mathrm{s}} \right|^2 \right\rangle &= \frac{2N_c \mathsf{S}}{\pi k_\alpha |\mathbf{x}|} \sum_{m=-\infty}^{\infty} (\mathcal{A}_m)^2 \\
&\quad \times \int_{r'=0}^{r'=\infty} \int_{\phi'=0}^{\phi'=2\pi} N(r') \exp[i(m\phi' - k_{\alpha_1} r' \cos\phi')] r'\, dr'\, d\phi', \\
\left\langle \left| \Psi_a^{\mathrm{s}} \right|^2 \right\rangle &= \frac{2N_c \mathsf{S}}{\pi k_\beta |\mathbf{x}|} \sum_{m=-\infty}^{\infty} (\mathcal{B}_m)^2 \\
&\quad \times \int_{r'=0}^{r'=\infty} \int_{\phi'=0}^{\phi'=2\pi} N(r') \exp[i(m\phi' - k_{\beta_1} r' \cos\phi')] r'\, dr'\, d\phi'.
\end{aligned} \tag{18}$$

Here, note that the limit of the integral in r' is extended to $r' = \infty$ since we consider the distribution of heterogeneities to be sparse and homogeneous in the media. Thus, the value of $N(r')$ is small at a large offset (e.g. Frankel & Clayton 1986).

The integral of the exponential function in (18) can be rewritten in terms of Bessel functions and the integral with a Bessel function can be expressed by a Hankel transform $\mathcal{H}$ (Arfken 1985, p. 587, p. 795):

$$\begin{aligned}
&\int_0^{2\pi} \exp[i(x\cos\phi' + m\phi')]\, d\phi' = i^m 2\,(x), \\
&\mathcal{H}_m(k) = \mathcal{H}[m, N(r'); k] = \int_0^{\infty} N(r') r' J_m(kr')\, dr',
\end{aligned} \tag{19}$$

where $J_m(x)$ is the mth order of Bessel function and $\mathcal{H}_m(k)$ is the Hankel-transformed autocorrelation function $[N(r')]$. Note that the Hankel transform is equivalent to a 2-D Fourier transform when $m = 0$, and $\mathcal{H}_0(k_j)$ is a power spectral density function, the spectrum of $N(r')$. Thus,

$\langle|\Phi_a^s|^2\rangle$ and $\langle|\Psi_a^s|^2\rangle$ in (18) are given by

$$\left\langle\left|\Phi_a^s\right|^2\right\rangle = \frac{4N_c\mathsf{S}}{k_\alpha|\mathbf{x}|}\sum_{m=-\infty}^{\infty}(\mathcal{A}_m)^2\mathcal{H}_m(-k_\alpha),$$

$$\left\langle\left|\Psi_a^s\right|^2\right\rangle = \frac{4N_c\mathsf{S}}{k_\beta|\mathbf{x}|}\sum_{m=-\infty}^{\infty}(\mathcal{B}_m)^2\mathcal{H}_m(-k_\beta). \tag{20}$$

The attenuation rate (Q^{-1}) corresponds to the energy loss per unit area divided by the solid angle (2π) and the wavenumber of incident waves. Therefore, the attenuation rate Q^{-1} over a spatial lag r is given by

$$Q^{-1} = \frac{N_c r}{2\pi\mathsf{S}k_\alpha}\left\{\left\langle\left|\Phi_a^s\right|^2\right\rangle + \frac{1}{\gamma}\left\langle|\Psi_a^s|^2\right\rangle\right\}, \tag{21}$$

where $\gamma = \alpha/\beta = k_\beta/k_\alpha$. N_c can also be expressed as the multiplication of the area of the cavity zone (A_c) and the number density (η), i.e. $N_c = \eta\,\mathsf{A}_c$. Therefore, the theoretical scattering attenuation variation for media bearing randomly distributed cavities with number density η is given by (Hong & Kennett 2003a; Hong 2004)

$$\frac{Q^{-1}}{\eta} = \frac{2\mathsf{A}_c}{\pi k_\alpha^2}\left\{\sum_{m=-\infty}^{\infty}(\mathcal{A}_m)^2\mathcal{H}_m(-k_\alpha)\right\} + \frac{2\mathsf{A}_c}{\pi k_\beta^2}\left\{\sum_{m=-\infty}^{\infty}(\mathcal{B}_m)^2\mathcal{H}_m(-k_\beta)\right\}. \tag{22}$$

Note that, when we consider the scattering attenuation problems with constant incident waves in media with different scales of cavities, the scaling factors ($2\mathsf{A}_c/\pi k_\alpha^2$, $2\mathsf{A}_c/\pi k_\beta^2$) and the Hankel-transform values ($\mathcal{H}_m$) are determined constant. Therefore, the variation of scattering attenuation is dependent on the variation of coefficients $\mathcal{A}_m$ and $\mathcal{B}_m$, which are roughly proportional to the normalized wavenumbers ($k_\alpha a_c$, $k_\beta a_c$). On the other hand, when the variation of scattering attenuation is investigated for a change of the frequency content of incident waves in a medium with a constant scale of cavities, the scattering attenuation will be more dependent on the scaling factors than the coefficients (note that, angular frequency = wavenumber × velocity). Therefore, they will decrease with the incident-wave frequency (i.e. with normalized wavenumber).

It is noteworthy that the scattering attenuation in stochastic random media, which have continuous and gradually varying perturbation, varies with the value of normalized wavenumber. Thus, for the scattering in stochastic random media, a change of heterogeneity scale is equivalent to a change of incident-wave frequencies. However, the parameter influence on scattering attenuation in cavity-based media is different between the cavity scale and the incident-wave frequency. Detailed description of scattering attenuation properties in media with cavities is made in Section 5.

The theoretical scattering attenuation expression (22) can be applied to media with any cavities, which may be filled with vacuum, fluid, or elastic material. Different filling materials of cavities can be considered by implementing appropriate coefficients A_m and B_m in (4) which account for the physical properties of the media. The theoretical scattering attenuation expression is based assumptions that cavities are distributed uniformly and randomly in a medium and the distances between cavities are sufficiently large. Under these assumptions, the single scattering effect is the dominant factor influencing the scattering energy loss of primary waves. Thus, the theoretical prediction may not be applicable to problems with a large scale and number of cavities, where the multi-scattering effect is not negligible. That is, the theoretical prediction may be effective in a medium of $\pi N_c a_c^2 \ll A_c$.

4 DETERMINATION OF THE AUTOCORRELATION FUNCTION

For the computation of theoretical scattering attenuation variation in media with randomly distributed cavities from (22), it is required first to determine the autocorrelation function (ACF) $N(r)$ in the spatial domain. We determine $N(r)$ empirically through numerical experiments in media with various number densities ($\eta = 0.05, 0.2, 0.5, 0.8, 1.0$). The location map $R(\mathbf{x})$ in (10) corresponds to the locations of cavities in media, and is represented by a collection of delta functions distributed in the spatial domain. Thus, the autocorrelation values of the delta functions can be determined numerically by (*cf.* Roth & Korn 1993)

$$U(r) = \langle R(\mathbf{x})R(\mathbf{y})\rangle = \frac{1}{r_{\max}}\int_0^{r_{\max}} R(r')R(r+r')\,dr', \tag{23}$$

where $r_{\max}$ is the maximum spatial lag in the medium. Here $U(r)$ represents unnormalized autocorrelation values, which are dependent on the number density (η) of the medium. The unnormalized autocorrelation value can be expressed in terms of the normalized autocorrelation value $N(r)$:

$$U(r) = \eta N(r). \tag{24}$$

The representative autocorrelation function can be implemented for problems with any number densities.

The autocorrelation values should be determined constant despite the change of the number of gridpoints as long as the number density is identical. Note that the change in the number of grid points causes a difference in the resolution of domain representation. We thus compare numerical autocorrelation values from two different sizes of domains; 50-by-50 and 100-by-100 grid points (Fig. 7). For normalization in distance, we introduce a relative distance r/l where l is the reference distance (e.g. vertical or horizontal length of the medium). The estimated

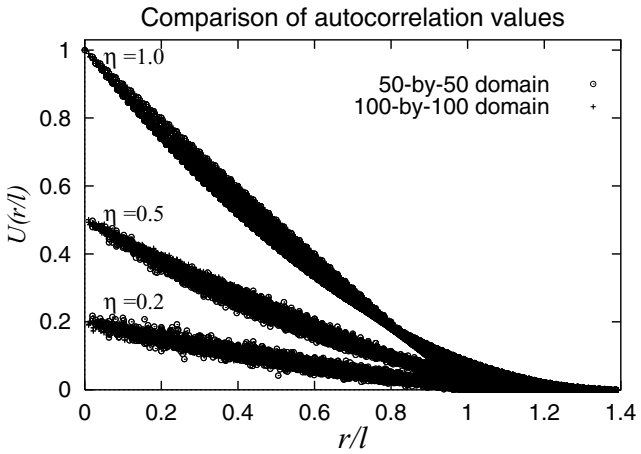

Figure 7. Estimated autocorrelation values of $R(\mathbf{x})$ for three number densities ($\eta = 0.2, 0.5, 1.0$) in 50-by-50 and 100-by-100 gridpoint domains. The estimated values of the two domains are very close.

autocorrelation values of both experiments are very close. But the results from a 100-by-100 gridpoint domain show a more confined trend, since the variation of autocorrelation values with spatial distance is resolved better due to the decrease of grid-step size. Fig. 7 shows that the autocorrelation values are proportional to the number density as indicated in (24).

For the representation of numerical autocorrelation values, polynomials or single functions can be considered. However, several analytic functional pairs of Hankel transform are reported (Sneddon 1972), and thus it is usually very difficult to obtain the Hankel-transformed outputs ($\mathcal{H}_m$ in (20), $m =$ integer) of arbitrary functions. Moreover, the numerical computation of Hankel transform, which is used popularly in electromagnetic modelling (Anderson 1984), is restricted to lower orders of m (i.e. $m = 0$, 1, see Anderson 1989). Only a few functions are known to have analytic forms for any orders of m, and the Gaussian (e^{-pr^2}) and exponential functions (e^{-pr}) look appropriate for the basis functions of polynomials for the representation of numerical autocorrelation values. The Hankel-transformed outputs of the Gaussian and the exponential functions are

$$\mathcal{H}(m, e^{-pr}; k) = k^m (p^2 + k^2)^{-\frac{3}{2}} (p + m\sqrt{p^2 + k^2})(p + \sqrt{p^2 + k^2})^{-m}, \tag{25}$$

and

$$\mathcal{H}(m, e^{-pr^2}; k) = \frac{k^m \Gamma\left(\frac{1}{2}m + 1\right)}{2^{m+1} p^{\frac{1}{2}m+1} \Gamma(m+1)} \times {}_1F_1\left(\frac{1}{2}m + 1; m + 1; -\frac{k^2}{4p}\right), \tag{26}$$

where p is a constant, Γ is the Gamma function, and ${}_1F_1$ is the confluent hypergeometric function defined as

$${}_1F_1(g; h; x) = \sum_{n=0}^{\infty} \frac{(g)_n}{n!(h)_n} x^n, \tag{27}$$

and $(g)_n = g(g+1)(g+n-1)$.

In this study, we employ a polynomial composed of exponential functions:

$$N(r) = \sum_{n=1}^{N_p} a_n \exp(-b_n r), \quad (b_n > 0), \tag{28}$$

where r/l is the normalized distance and a_n and b_n are constant coefficients to be determined by a least-squares fitting. It is obvious that, when the more functions are implemented, the better fitting can be achieved for a given data set. However, the representative function for autocorrelation values should be determined so that it satisfies also the general features expected in spatial domain. For instance, autocorrelation values should decrease with spatial lag, but they should not be negative values. Empirically, it is found that the ACFs represented by polynomials with many functions often display negative values at a large spatial distance, outside the range of the data set, although they stand for the data well within the data set range. This is because the set of coefficients a_n is determined to be mixture of positive and negative values when a large number of functions are implemented. The coefficients a_n, thus, are required to be positive values in order to satisfy the expected trend. We find that polynomials with two basic functions are sufficient for the representation of autocorrelation values. Fig. 8 shows a comparison between two estimated ACFs; one ACF is composed of two exponential functions and the other is of five exponential functions. The ACF based on five exponential function displays negative values at a large distance outside the data set, while the other ACF exhibits a reasonable trend.

The coefficients a_n and b_n in (28) for ACF with two exponential functions (i.e. $N_p = 2$) are determined as

$$a_1 = 0.982, \quad a_2 = 0.397, \quad b_1 = 2.2, \quad b_2 = 4. \tag{29}$$

The comparisons between numerical values and the estimated ACF ($U(r/l)$) in Fig. 9 display a good fit for the data set with small number densities ($\eta = 0.05$, 0.2), but rather poor agreement for those with large number densities ($\eta = 0.5$, 0.8, 1.0). Since, however, the area of

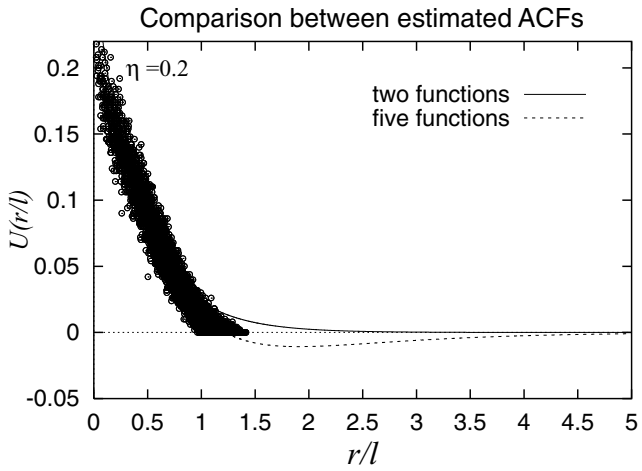

Figure 8. Comparison of ACFs composed of two and five exponential functions for a data set with $\eta = 0.2$. Both ACFs satisfy the data set well, but the ACF with five basis functions display unreasonable negative values at $r/l > 1.5$.

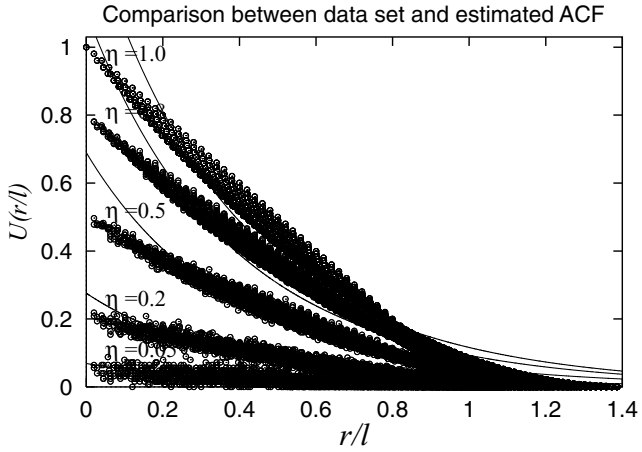

Figure 9. Comparisons between data sets and ACF based on two-exponential functions when $\eta = 0.05$, 0.2, 0.5, 0.8 and 1.0. The ACF satisfies the data sets for $\eta = 0.05$, 0.2 well, but become worse for the data sets with large η.

the cavity zone should be much larger than the area occupied by cavities (i.e. $A_c \gg N_c \pi a_c^2$, see Section 3) and N_c is expected to be small ($N_c < 0.001$ in this study), the estimated ACF is sufficient enough for practical application. From (25) and (28), the Hankel transform of the estimated ACF in (22) is given by

$$\mathcal{H}_m(k) = \mathcal{H}[m, N(r); k]$$
$$= k^m \sum_{n=1}^{N_p} a_n \left(b_n^2 + k^2\right)^{-\frac{3}{2}} \left(b_n + m\sqrt{b_n^2 + k^2}\right)\left(b_n + \sqrt{b_n^2 + k^2}\right)^{-m}. \quad (30)$$

We may employ an alternative polynomial composed of Gaussian-type exponential functions. However, although the Gaussian-type exponential function has its own analytic expression for the Hankel transform, it is often difficult to calculate the hypergeometric function ($_1F_1$) in (26) due to its slow convergence to the accurate value.

5 SCATTERING ATTENUATION

Stacked spectral amplitudes of primary waves are used for the measurement of scattering attenuation. Here, in order to exclude the influence of scattered waves from the spectral amplitude of primary waves, we select only the primary-wave portion from every time response using an adaptive time window based on a cosine bell before the staking of spectral amplitudes (see Hong & Kennett 2003a). The amplitude stacking in a Fourier space allows us to determine the primary-wave amplitude correctly without overestimation of energy loss by the traveltime fluctuation, which is required to be corrected in a time-domain stacking (Roth & Korn 1993; Sato & Fehler 1998; Hong & Kennett 2003a). The size of the adaptive time window varies $1.2T_p$ to $1.4T_p$, where T_p is the period of the primary waves.

Fig. 10 shows the stacked spectral amplitudes of several models with fluid-filled cavities. Spectral amplitudes of x components are provided in the figure for a comparison with those of z components. The spectral amplitudes of the primary wave, which are shown in z

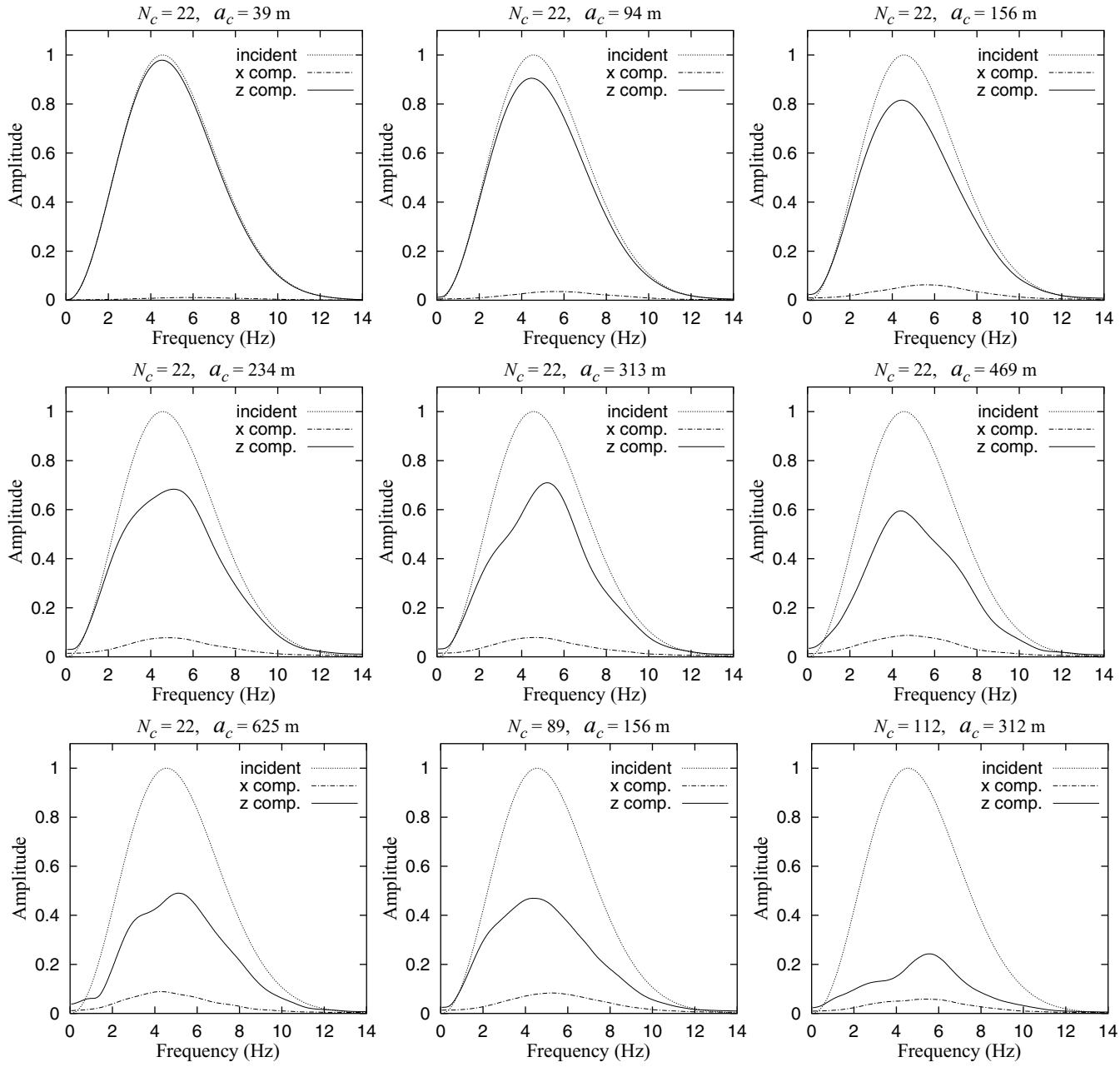

Figure 10. Spectral amplitudes of time responses in x and z components. For the reference, the spectral amplitudes of incident waves are provided. Energy dissipation is proportional to the number of cavities and the size of radius. Spectral amplitudes in x components are nearly invariant for the change of spectral amplitudes in z components.

components, decrease with the number (N_c) and the scale (a_c) of cavities. On the other hand, the spectral amplitudes of x components are nearly invariant with the change of spectral amplitudes at z components when N_c and a_c are large. This implies that the primary waves are recorded mainly at z components, which correspond to the initial polarization direction of incident waves. On the other hand, the wave train in x component is composed mainly of scattered waves. Note that scattered waves develop on the cavity boundaries, where sharp transition in physical properties is made, and are distributed uniformly over a space. Also, as shown in Section 2, the energy loss by the scattering at cavities are evenly distributed over the entire primary wave front by a continuous phase healing process during propagation.

The primary wave fronts are composed partly of the forward diffracted waves, which keep a pace with adjacent primary waves and are recorded mostly at z components. However, the backward and sideward diffracted waves and multi-scattered (or, multi-reflected) waves hardly contribute to the construction of primary wave front. Thus, the primary waves are recorded mostly at z components, and the scattering attenuation rates can be measured through a single-component analysis which assesses the energy recorded at the components in the polarization direction. These scattering features are different from those found in stochastic random media, where primary waves are recorded also in the orthogonal components due to the deviation of the propagation direction of primary wave from the incidence direction by the interference

with the continuous and gradually varying stochastic random heterogeneities (Hong & Kennett 2003a). Thus, for the correct measurement of scattering attenuation in stochastic random media, a multi-component analysis is required (Hong & Kennett 2003a). The multi-component analysis is important especially when the correlation length is large, since the deviation rate of propagation direction increases with the correlation distance.

The theoretical scattering attenuation variation with normalized wavenumber ($k_\alpha a_c$) is obtained from (22). The scattering attenuation rates of synthetic data are measured using the stacked spectral amplitude of time responses from a formula of Aki & Richards (1980):

$$Q^{-1}(\omega) = \frac{2\alpha_0}{\omega r} \ln\left[\frac{A_0(\omega)}{A_r(\omega)}\right], \tag{31}$$

where α_0 is the vertically incident P-wave velocity, r is the vertical length of the cavity zone, ω is the angular frequency, and $A_0(\omega)$ and $A_r(\omega)$ are the stacked spectral amplitudes of primary waves at the origin and the receiver. The spectral amplitudes in a frequency range of 2–10 Hz are applied for the measurement of scattering attenuation. Note that the dominant frequency of incident waves is 4.5 Hz.

We investigate the variation of scattering attenuation for a case with a constant wavenumber and varying cavity scales and for a case with constant cavity scales and varying wavenumbers. We first consider the cases with varying cavity scales using the synthetic data of various models in Section 2. The value of dominant frequency (4.5 Hz) is used for the computation of theoretical scattering attenuation rates. In Fig. 11, the predicted and estimated scattering attenuation rates increase with cavity scales, as expected in Section 3. Note that each numerical estimate is measured in a frequency range of 2–10 Hz and the theoretical curve is for a case of constant incident-wave frequency, 4.5 Hz.

The slope of the theoretical scattering attenuation curve for constant k_α and varying a_c, however, is not constant over the whole range, but can be divided into several segments. In particular, the slope at $k_\alpha a_c > 10^{1.3}$ is nearly zero, which means that the primary waves are expected to be exhausted mostly under this single-scattering theory. The increase of scattering attenuation with the cavity scale is related to the fact that the scattering area (i.e. the surfaces of cavities) increases with the cavity scale and also the traveltime difference between the forward diffracted waves and the cavity-transmitted waves (waves transmitting through cavities) becomes large with the cavity scale. Thus, the influence by cavity-transmitted waves on the construction of primary wave front is weakened with increase of cavity scale. Consequently, the energy loss increases with the cavity scale and decreases with the frequency of incident waves. However, considering that the theoretical prediction is based on a single scattering theory which ignores the effect of multiscattering between cavities, the theoretical prediction can be an overestimate in a medium with a large scale and number of cavities.

In Fig. 11, the solid lines represent the results from models with 22 cavities and the open circles are for models with 89 or 112 cavities. The variation of numerical estimates with cavity scales agrees well with the theoretical prediction. In particular, the normalized attenuation rates (Q^{-1}/η) from media with 89 and 112 cavities coincide with those from media with 22 cavities with the same radii (i.e. $a_c = 156$, 312 m). This indicates that the scattering attenuation rates are proportional to the number density (η) and the energy loss of primary waves is influenced mainly by the first-order scattered waves.

The scattering attenuations from each numerical experiment display that they decrease with a frequency but increase with a cavity scale. This characteristic feature agrees with the theoretical expectation in Section 3. The decrease of scattering attenuation with frequency conforms to the general pattern found in field observations (Yoshimoto *et al.* 1998) and numerical studies (Benites *et al.* 1992). In Fig. 12, we now show the variation of scattering attenuation with frequency for given cavity scales. The theoretical curves are computed also from (22) by changing

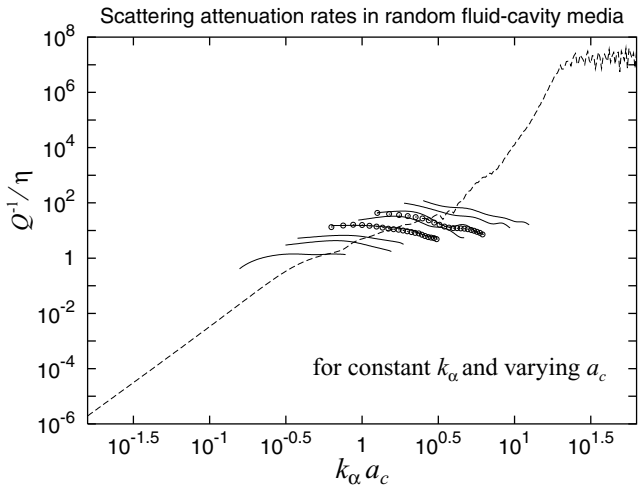

Figure 11. Comparisons of scattering attenuation rates between numerical estimates and the theoretical variation for a change of cavity scale. The cavity scales (a_c) in numerical models are 39 m, 78 m, 94 m, 156 m, 234 m, 312 m, 468 m and 625 m. The numerical estimates with solid lines are from media with 22 cavities, and those with open circles are from media with different numbers (89 and 112) of cavities. The numerical estimates are measured in a frequency range of 2–10 Hz, and the theoretical curve is computed using the dominant frequency of incident waves (4.5 Hz). The numerical estimates agree with the theoretical trend.

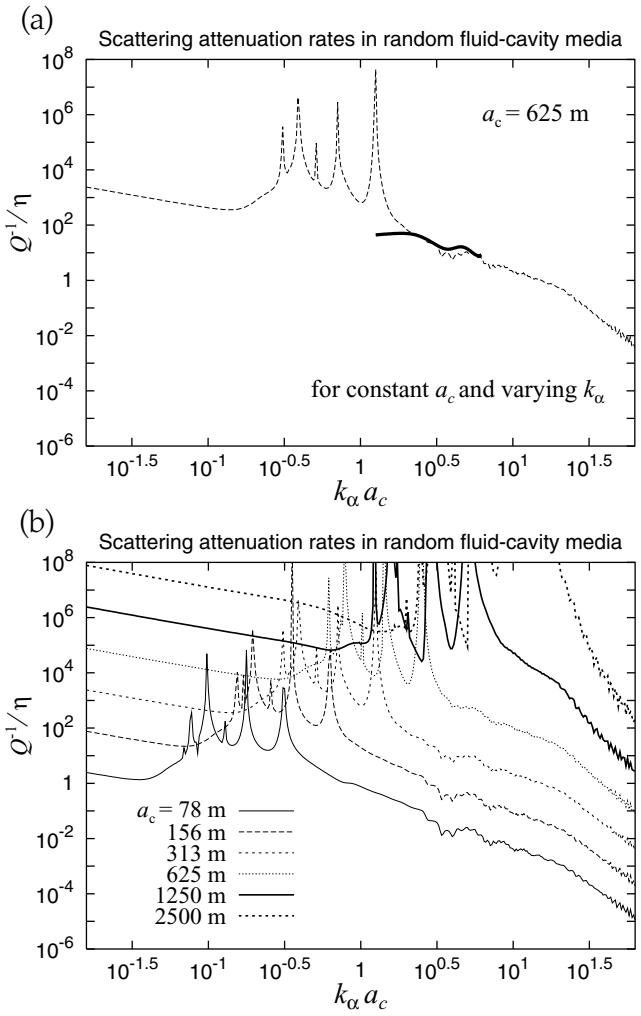

Figure 12. (a) A comparison of scattering attenuation between numerical estimates and the theoretical variation for the change of frequency (wavenumber) at $a_c = 625$ m. The numerical estimates agree well with the theoretical prediction. (b) Comparisons of theoretical scattering attenuation variation with the change of frequency for different cavity scales. The change of the cavity scale causes a change in scattering attenuation level over the entire $k_\alpha a_c$ range, and the level of scattering attenuation is proportional to the cavity scale.

the incident-wave frequency instead of the cavity scale. The theoretical scattering attenuation curves agree well with numerical estimates for $a_c = 625$ m (Fig. 12a).

The rapid fluctuation in the theoretical curves looks to be related with the numerical difficulty in computation of the Hankel-transforms ($\mathcal{H}_m$). A selection of a different scale of cavities causes a change in scattering attenuation level in the entire $k_\alpha a_c$ range, but the general trend of scattering attenuation with frequency is nearly consistent (Fig. 12b). Thus, a high level of attenuation is expected when waves are incident to a medium with a large scale of cavities, and the scattering attenuation is strengthened when low-frequency waves are incident.

The characteristic parameter dependence of scattering attenuation in cavity-based media is quite different from that in stochastic random media. Note that, in stochastic random media, scattering attenuation varies with the value of normalized wavenumber (ka), thus the influence by a change in heterogeneity scale is equivalent to that by a change in frequency (wavenumber). The variation pattern of scattering attenuation with frequency also looks different between the two types of media. The stochastic random media show a pattern that scattering attenuations increase until around $ka = 1$ and then decrease with ka. On the other hand, the scattering attenuations in cavity-based media rather decrease with $k_\alpha a_c$ over the whole range. So, it appears that scattering pattern in media with heterogeneities with high physical impedance contrast may not be well represented using a stochastic random model.

6 DISCUSSION AND CONCLUSIONS

Random heterogeneities with high physical impedance were implemented for an alternative representation of random heterogeneities, and the scattering properties in media with the heterogeneities were investigated. Fluid-filled circular cavities are considered for the representation of random heterogeneities.

The amplitudes of primary waves recorded in time responses becomes smaller with increase of the size of cavities. However, the decrease of energy in the primary-wave portion scarcely causes the increase of scattered waves in time responses when the size of cavities is large. The backscattered waves and the trapped waves inside cavities increase with the size of cavities, and so they scarcely reach receivers placed beyond the cavity zone and hardly attribute to coda waves. Therefore, the level of total energy in time response becomes weaker with the size of cavities. On the other hand, the energy decrease in primary waves causes an increase of coda-wave level in stochastic random media (Hong & Kennett 2003a).

The Primary wave front, which is built in a cavity zone, is composed of forward diffracted waves, transmitting waves through cavities, and the complementary energy from adjacent primary waves via the wave front healing effect. Here, the influence of the transmitting waves through cavities is weakened in media with a large scale of fluid-filled cavities due to the increase of traveltime difference. Also, the forward diffracted waves propagating with a large angle from the incidence angle does not join with the primary-wave portion for the same reason. Thus, the propagation direction of primary waves in random cavity media is very close to the incidence direction, and primary waves are recorded mainly on z components. However in stochastic random media with large correlation lengths, primary wave front used to deviate from the incidence direction and a significant energy of the primary waves is observed in the orthogonal components (i.e. x components). Therefore, a dual-component analysis is essential for the estimation of scattering attenuation rates (see Hong & Kennett 2003a).

A theoretical scattering attenuation expression based a single scattering theory was formulated for media with randomly distributed circular cavities. Any materials inside the cavities can be considered in the theory through implementation of appropriate reflection and transmission coefficients for boundary conditions on the surface of cavities. The autocorrelation function for the representation of cavity distribution in spatial domain, was determined numerically using a polynomial composed of two exponential functions. The autocorrelation function can be determined with other sets of functions.

Numerical estimates of attenuation rates agree well with the theoretical attenuation variation. The scattering attenuation rates are proportional to the number density (η), but the normalized attenuation rates (Q^{-1}/η) are determined very close for different number densities The scattering attenuation in the cavity-based media shows a characteristic parameter dependency for frequency (wavenumber) and cavity scale. The scattering attenuation increases with the cavity scale, while it decreases with the frequency content of incident waves. This property is different from that found in stochastic random media where scattering attenuation is determined by the value of normalized wavenumber (ka). Thus, a reciprocal feature is established between the wavenumber and heterogeneity scale in the scattering at stochastic random media, while that is not hold in the scattering at the cavity-based media. Also, the frequency-dependent variation of scattering attenuation is displayed different between the two types of media. Consequently, the scattering properties are very different between the cavity-based media and stochastic random media. Thus, for the description of highly impeditive heterogeneities in the earth, it appears to be desirable to use both a model with discrete heterogeneities and a stochastic random model with continuous variation.

The wavelet-based method provides stable time responses in media composed of random heterogeneities with high physical impedance and allows a quantitative seismic study in numerically challenging problems.

ACKNOWLEDGMENTS

We are grateful to Professor Michael Korn and two anonymous reviewers for the constructive review comments. We acknowledge the Australian National University Supercomputer Facility for allocation of computational time in the Alpha server.

REFERENCES

Aki, K. & Richards, P.G., 1980. Quantitative Seismology, Theory and Methods, Volume 1. W.H. Freeman, San Francisco.

Anderson, W.L., 1984. Computation of Green's tensor integrals for three-dimensional electromagnetic problems using fast Hankel transforms, *Geophysics,* **49,** 1754–1759.

Anderson, W.L., 1989. A hybrid fast Hankel transform algorithm for electromagnetic modelling, *Geophysics,* **54,** 263–266.

Arfken, G., 1985. *Mathematical Methods for Physicists,* 3rd edn, Academic Press, New York.

Benites, R., Aki, K. & Yomogida, K., 1992. Multiple scattering of *SH* waves in 2-D media with many cavities, *Pure appl. Geophys.,* **138,** 353–390.

Carcione, J.M., 1998. Scattering of elastic waves by a plane crack of finite width in a transversely isotropic medium, *Int. J. Num. Anal. Meth.,* **22,** 263–275.

Chernov, L.A., 1960. *Wave Propagation in a Random Medium,* McGraw-Hill Book Company, Inc., New York.

Coutant, O., 1989. Numerical study of the diffraction of elastic waves by fluid-filled cracks, *J. geophys. Res.,* **94,** 17 805–17 818.

Frankel, A. & Clayton, R., 1986. Finite difference simulation of seismic scattering: Implications for the propagation of short-period seismic waves in the crust and models in crustal heterogeneity, *J. geophys. Res.,* **91,** 6465–6489.

Haskell, N.A., 1953. The dispersion of surface waves on multilayered media, *Bull. seism. Soc. Am.,* **43,** 17–34.

Hong, T.-K., 2004. Scattering attenuation ratios of *P* and *S* waves in elastic media, *Geophys. J. Int.,* **158,** 211–224.

Hong, T.-K. & Kennett, B.L.N., 2002a. A wavelet-based method for simulation of two-dimensional elastic wave propagation, *Geophys. J. Int.,* **150,** 610–638.

Hong, T.-K. & Kennett, B.L.N., 2002b. On a wavelet-based method for the numerical simulation of wave propagation, *J. Comput. Phys.,* **183,** 577–622.

Hong, T.-K. & Kennett, B.L.N., 2003a. Scattering attenuation of 2D elastic waves: theory and numerical modeling using a wavelet-based method, *Bull. seism. Soc. Am.,* **93**(2), 922–938.

Hong, T.-K. & Kennett, B.L.N., 2003b. Modelling of seismic waves in heterogeneous media using a wavelet-based method: application to fault and subduction zones, *Geophys. J. Int.,* **154,** 483–498.

Hudson, J.A., 1980. Overall properties of a cracked solid, *Math. Proc. Camb. Phil. Soc.,* **88,** 371–384.

Igel, H. & Gudmundsson, O., 1997. Frequency-dependent effects on travel times and waveforms of long-period *S* waves: Implications for the scale of mantle heterogeneity, *Phys. Earth Planet. Int.,* **104,** 229–246.

Kawahara, J. & Yamashita, T., 1992. Scattering of elastic waves by a fracture zone containing randomly distributed cracks, *Pure appl. Geophys.,* **139,** 121–144.

Liu, E., Crampin, S. & Hudson, J.A., 1997. Diffraction of seismic waves by cracks with application to hydraulic fracturing, *Geophysics,* **62,** 253–265.

Liu, Y., Wu, R.-S. & Ying, C.F., 2000. Scattering of elastic waves by an elastic or viscoelastic cylinder, *Geophys. J. Int.,* **142,** 439–460.

Murai, Y., Kawahara, J. & Yamashita, T., 1995. Multiple scattering of *SH* waves in 2-D elastic media with distributed cracks, *Geophys. J. Int.,* **122,** 925–937.

Nagano, K., 1998. Crack-wave dispersion at a fluid-filled fracture with low-velocity layers, *Geophys. J. Int.,* **134,** 903–910.

Pao, Y.-H. & Mow, C.-C., 1973. *Diffraction of Elastic Waves and Dynamic Stress Concentrations,* Crane, Russak & Compa, New York.

Pointer, T., Liu, E. & Hudson, J.A., 1998. Numerical modelling of seismic waves scattered by hydrofractures: application of the indirect boundary element method, *Geophys. J. Int.,* **135,** 289–303.

Roth, M. & Korn, M., 1993. Single scattering theory versus numerical modelling in 2-D random media, *Geophy. J. Int.,* **112,** 124–140.

Sato, H. & Fehler, M.C., 1998. *Seismic Wave Propagation and Scattering in the Heterogeneous Earth,* Springer-Verlag, New York.

Sneddon, I.N., 1972. *The Use of Integral Transforms,* McGraw-Hill, Inc., New York.

Wu, R.-S., 1982. Attenuation of short period seismic waves due to scattering, *Geophys. Res. Lett.,* **9,** 9–12.

Yomogida, K. & Benites, R., 1995. Relation between direct wave *Q* and coda *Q*: A numerical approach, *Geophys. J. Int.,* **123,** 471–483.

Yomogida, K. & Benites, R., 2002. Scattering of seismic waves by cracks with the boundary integral method, *Pure appl. Geophys.,* **159,** 1771–1789.

Yoshimoto, K., Sato, H., Iio, Y., Ito, H., Ohminato, T. & Ohtake, M., 1998. Frequency-dependent attenuation of high-frequency *P* and *S* waves in the upper crust in western Nagano, Japan, *Pure appl. Geophys.,* **153,** 489–502.